PHOTOLUMINESCENCE MAPPING OF OPTICAL DEFECTS IN HPHT SYNTHETIC DIAMOND

Lorne C. Loudin

Photoluminescence (PL) mapping provides a means to identify the distribution of optical centers in diamond. To demonstrate the impact of this method on the field of gemology and the study of diamonds, photoluminescence maps were acquired from a laboratory-irradiated brownish orange HPHT synthetic diamond of mixed diamond type. Acquisition time for each PL map was less than four minutes. Analysis of the maps confirmed that optical centers are incorporated in diamond growth sectors, such as {111} octahedral, {100} cubic, {110} dodecahedral, and {113} trapezohedral. The remarkable correlation between optical defects and growth sectors in the sample demonstrates that high-speed photoluminescence mapping is ideal for rapidly determining the distribution of optical defects resulting from both diamond growth and treatments. We anticipate that this technique will allow gemological labs to continue to identify increasingly sophisticated synthetic diamonds and color treatments, helping to ensure consumer confidence in the diamond industry.

In Brief

- Photoluminescence mapping provides an additional tool for gemological laboratories to identify diamond synthetics and color treatments.
- A Raman imaging microscope with an electron-multiplying charge-coupled device can produce PL maps that reveal the spatial distribution of optical defects.
- Analysis of PL maps also reveals information about the nature and formation of these optical defects.

Optical centers in a diamond's crystal lattice, also known as point defects, absorb visible light to produce color (Collins, 1982). In this way, optical centers give rise to the variety of fancy-color diamonds available in the trade. Optical centers can form as a result of impurities in the diamond (such as nitrogen or boron), deformation of the crystal lattice, missing carbon atoms (vacancies), or a combination of these (Collins, 2003; Breeding and Shigley, 2009). Photoluminescence occurs when an optical center is excited to a higher energy state by the absorption of photons and then returns to its ground energy state, emitting light at a specific wavelength or band of wavelengths (Collins, 1992; Eaton-Magaña and Breeding, 2016). There are currently several hundred known optical centers in diamond that produce photoluminescence (e.g., Collins, 1999; Zaitsev, 2001).

Photoluminescence (PL) spectroscopy is a powerful tool used in gemological laboratories to verify whether a specimen is natural or synthetic and determine whether its color origin is natural or due to treatment (Eaton-Magaña and Breeding, 2016). One drawback is that spectra are often collected from a single spot, or a few spots, on the sample surface and therefore represent only a tiny fraction of the entire sample (figure 1). In general, the spectra collected are sufficient for a trained gemologist to determine the diamond's origin, especially when the PL spectra are interpreted in concert with DiamondView images, Fourier-transform infrared (FTIR) spectra, and other absorption and luminescence data. However, as synthetic diamond technology improves for both HPHT- and CVD-grown diamonds (e.g., Moe et al., 2016; Wang and Poon, 2016; Law and Wang, 2016; Eaton-Magaña and Shigley, 2016), and color treatments advance (e.g., Moe et al., 2015; Ardon and Loudin, 2016), gemological laboratories must introduce new techniques to continue to identify all synthetic and treated diamonds.

See end of article for About the Author and Acknowledgments.
GEMS & GEMOLOGY, Vol. 53, No. 2, pp. 180–188,
http://dx.doi.org/10.5741/GEMS.53.2.180

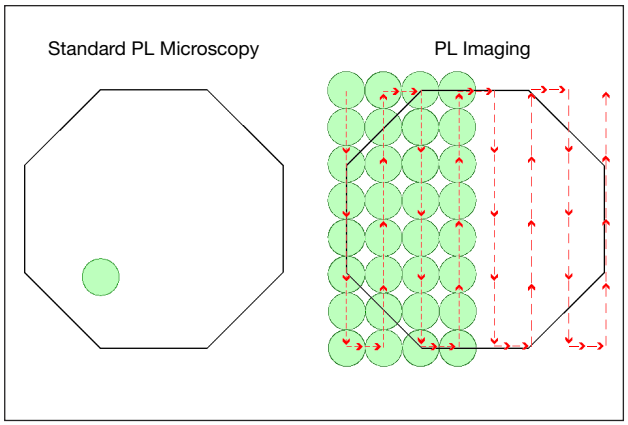

Figure 1. Schematic representation comparing PL methods. With standard PL microscopy, a single spot (shown as a green circle in the figure) is analyzed and represents only a small volume of the actual sample. With PL mapping, numerous spots are collected in a raster pattern (indicated by the dashed red arrows on the right), and the data are interpolated and combined to produce a PL map. Spot size is not to scale.

One useful technique is PL mapping (Eaton-Magaña and Breeding, 2016), which can be used to plot the distribution of an optical defect's intensity. A PL mapping microscope can collect thousands of spectra in a raster pattern by either continuously scanning the sample's surface or by moving from one point to another (pixel to pixel) and collecting a spectrum at each point. The spectral data are then interpolated and combined to produce a map of a defect's distribution (again, see figure 1). PL mapping was first used for gemological purposes in the summer of 2015; the first public demonstration of the technique was by Johnson et al. (2015) at the annual Geological Society of America conference in Baltimore. The technique was further developed by Dieck et al. (2015) to show the distribution of the silicon vacancy (SiV^-) in a CVD synthetic diamond. Ardon and Loudin (2016) used PL mapping to show the influence of focused beam irradiation on the distribution of nitrogen vacancies. Most recently, Johnson and Myagkaya (2017) used PL mapping to show the relationship between SiV^- and Ni^+ in an HPHT synthetic diamond.

One major challenge to implementing a PL mapping technique is that PL emission is temperature dependent. Therefore, the diamond must be cooled to liquid nitrogen temperature (approximately 77 K, or –321°F) to produce sharp PL bands (Collins, 1982; Eaton-Magaña and Breeding, 2016). Overcoming this challenge requires that the diamond be cooled in either a cryogenic stage or an open bath of liquid nitrogen. If the open-bath cooling method is used, then a high-speed mapping technique is needed because the liquid nitrogen boils off and vaporizes at atmospheric temperature and pressure. Using a Raman imaging microscope equipped with an electron-multiplying charge-coupled device (EMCCD), we were able to efficiently produce PL maps in less than four minutes, allowing us to overcome the temperature/time constraints and evaluate the distribution of optical centers in our synthetic diamond sample. Here we present an introduction to PL mapping and demonstrate the technique's effectiveness by reporting the distribution of optical defects in an HPHT synthetic diamond.

MATERIALS AND METHODS

GIA's New York laboratory received an irradiated 1.06 ct Fancy Deep brownish orange HPHT synthetic diamond of mixed type (figure 2) for a synthetic colored diamond grading report. Absorption features typical of both type IIb and type Ib diamonds were observed in the specimen's infrared absorption spectrum (figure 3). The type IIb component, attributed to boron in the diamond lattice, was identified by absorptions at 2803 and 2930 cm^{-1}. The type Ib component, composed of isolated nitrogen in the form of C centers, was identified by

Figure 2. This irradiated 1.06 ct Fancy Deep brownish orange HPHT-grown synthetic diamond of mixed type was examined in the study. Photo by Towfiq Ahmed.

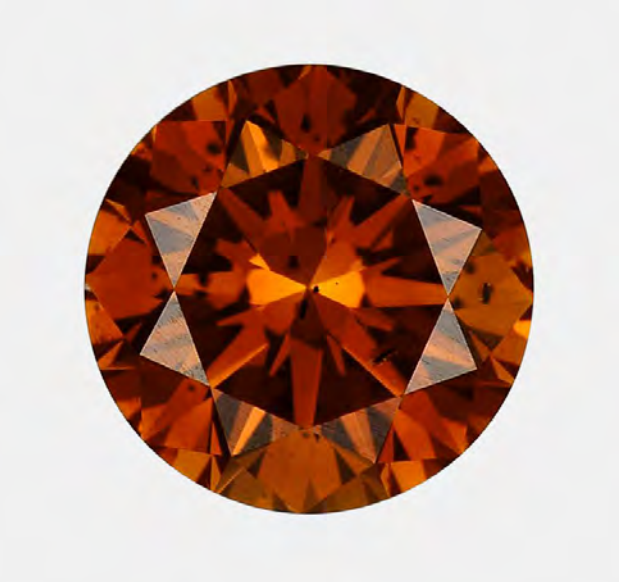

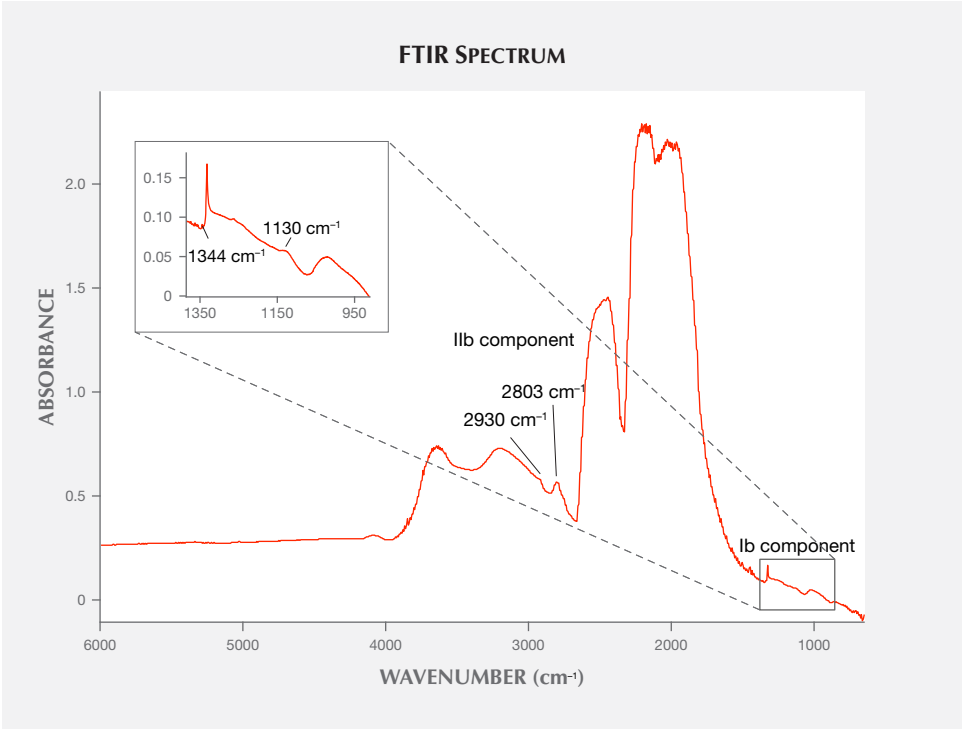

Figure 3. This FTIR spectrum showing both IIb and Ib (inset) peaks in the synthetic diamond sample.

infrared absorptions at 1130 and 1344 cm^{-1}. DiamondView images showed growth sectors corresponding to the {100} cubic, {111} octahedral, {110} dodecahedral, and {113} trapezohedral sectors (figure 4). PL spectra collected using a Renishaw inVia Raman microscope with 488, 514, and 830 nm laser excitation wavelengths revealed several PL features, including well-known defects such as NV^0 at 575 nm and NV^- at 637 nm, as well as several lesser-known defects such as 550.5 nm (figure 5). The combination of well-defined growth sectors and abundant optical defects made this sample well suited for demonstrating the effectiveness of PL imaging microscopy in mapping the distribution of optical defects in diamond.

PL mapping was performed at GIA's New York laboratory. Prior to mapping, the pavilion facets were coated with Pelco colloidal graphite to reduce the amount of light reflecting off the pavilion facet junctions and returning to the table. Additionally, the sample was mounted with the table level. Mapping was conducted using a Thermo Scientific DXRxi Raman imaging microscope with 455, 532, 633, and 780 nm laser excitation wavelengths. The DXRxi is equipped with an Olympus optical microscope and an Andor Technology Newton 970 EMCCD. An Olympus 10×, 0.25 numerical aperture objective lens was used.

The DXRxi uses a continuously moving, variable-speed sample stage driven by a combination of linear magnetic motors and controlled by optical encoders. The stage movement is synchronized with the

Figure 4. This DiamondView image of the synthetic diamond shows the {111}, {100}, {110}, and {113} growth sectors. For an overview of growth sector distribution in HPHT synthetic diamond, please see figure 5 in Welbourn et al. (1996).

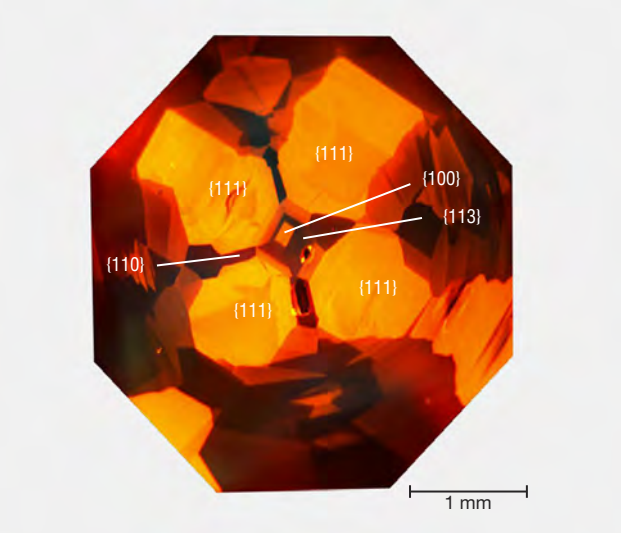

TABLE 1. Analytical conditions and Raman imaging microscope settings for each laser excitation wavelength.

	Laser wavelength (nm)			
	455	532	633	780
Grating (lines/mm)	1200	400	600	400
Laser power (mW)	5.9	0.3	8	24
Exposure time (ms)	1.67	1.67	1.67	8.33
Pinhole aperture size (μm)	50	25	50	50
Pixel size (μm)	15	15	15	25
EM gain	Off	Off	Off	Off
Total spectra	61,005	60,270	59,535	21,756
Collection time (min)	3.4	3.4	3.3	3.8

EMCCD detector exposures so that the spectra are collected at the desired positions with repeatability within 100 nm (A. Rzhevskii, pers. comm., 2016). For each laser excitation, the sample was analyzed at liquid nitrogen temperature to produce sharp PL peaks. The combination of an EMCCD detector and a variable-speed, exposure-synchronized stage allowed the DXRxi to produce high-quality PL maps while maintaining the appropriate temperature and level of liquid nitrogen. Table 1 summarizes the analytical conditions used for each laser excitation. The data were processed using Thermo Scientific's OMNICxi analysis software package, and baseline-corrected peak area profiles were used to produce the observed PL maps.

RESULTS

For each laser excitation wavelength, representative PL maps of the baseline-corrected peak area intensity are shown in figure 6. The maps are interpreted using a color scale. Warmer colors indicate a region that contains a greater intensity of a defect, while cooler colors represent lower intensities of that defect. The

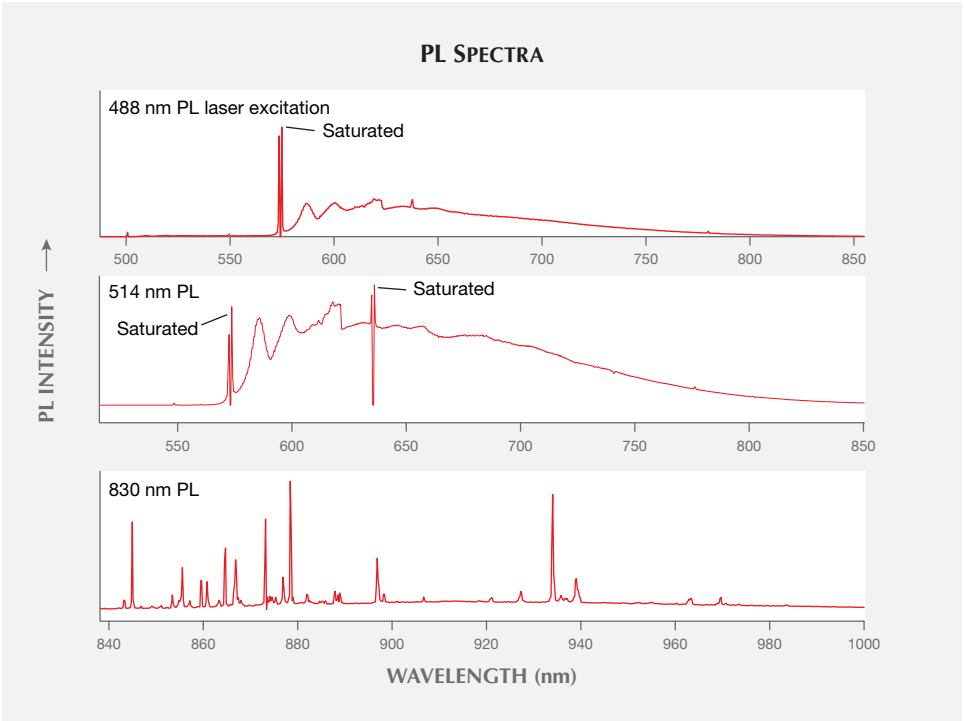

Figure 5. Note the variety of PL peaks in these photoluminescence spectra, specifically at 830 nm excitation.

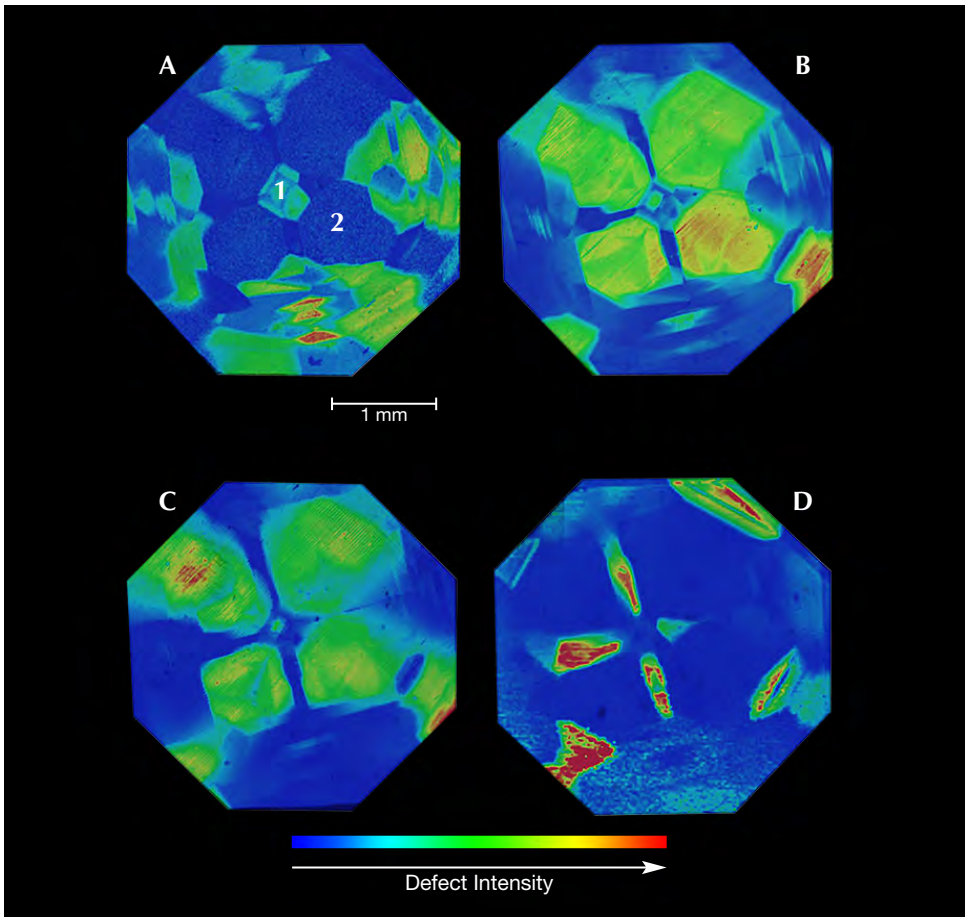

Figure 6. Representative PL images of the baseline-corrected peak area intensity for each laser excitation wavelength. A: The peak area distribution of the 508.8 nm peak (455 nm excitation). Points 1 and 2 represent the regions used for average spectra in figure 7. B: The peak area distribution of the 574.9 nm peak (532 nm excitation). C: The peak area distribution of the 637 nm peak (633 nm excitation). D: The peak area distribution of the 815.1 nm peak (780 nm excitation).

scale for each map depends on the defect's minimum and maximum intensity. To fully interpret the map, the spatial distribution of the defect must be taken in combination with the PL spectra. Figure 7 shows the average spectra from the {100} and {111} growth sectors around points 1 and 2 in figure 6A. Table 2 summarizes the peak area distribution per growth sector for a majority of the peaks observed in the DXRxi spectra. The data presented here are qualitative and are used for the purpose of demonstrating the technique.

The PL map in figure 6A, collected using the 455 nm laser, shows the peak area distribution of a band at 508.8 nm. The four growth sectors in the map—{100}, {111}, {110}, and {113}—correspond to those observed in the DiamondView image in figure 4. The peak area for the 508.8 nm band is greatest in the {100} sector, followed by {113} and {111}, respectively. The 508.8 band is undetectable in {110}. The same distribution is observed for the 470.1 nm peak. A band located at 506.1 nm displays a peak area distribution greatest in {113}; the band is also present in {110}, at approximately half the intensity in {113}. The remaining peaks listed in table 2 for the 455 nm laser were most intense in the {111} growth sector.

The relative peak area distributions for the 532 nm laser are summarized in table 2. Figure 6B shows the peak area distribution for the 575 nm PL band caused by NV^0. For NV^0, the {100}, {111}, {110}, and {113} growth sectors are all visible and correspond with the DiamondView image (again, see figure 4). The NV^0 band has the greatest peak area in the {111} growth sector, with the second-greatest intensity found in {100}. The NV^0 peak area is an order of magnitude lower in the {113} and {110} sectors than in {100}. The peak area distribution for NV^- at 637 nm follows a similar distribution. The peak area intensity of the NV^- center is approximately two times greater in the {111} sector than in {100}. The peak area for the GR1 defect at 741 nm was greatest in the {110} and {113} growth sectors; it was not present in the {111} and {100} sectors. Similar results for both NV^- and GR1 were observed in PL maps obtained using the 633 nm laser.

The peak area distribution for the NV^- center at 637 nm collected using the 633 nm laser is shown in figure 6C. Peak area distributions for the NV^- center

TABLE 2. Relative peak distribution per growth sector measured by the Raman imaging microscope using various laser excitation wavelengths.

Laser	Peak position (nm)	Peak intensity[a] per growth sector
455 nm	470.1	{100}>{113}>{111}>>{110}
	489.4	{111}≥{100}>>{113}
	490.2	{111}>{100}>{113}
	490.9	{111}≥{100}>{113}
	492.0	{111}≥{100}>{113}
	503.2	{111}≥{100}>{113}>>{110}
	506.1	{113}≥{110}
	508.8	{100}>{113}>{111}>>{110} (fig. 6A)
	517.6	{111}>>{110}
	537.8	{111}
532 nm	550.7	{111}>{100}
	574.9	{111}>{100}>>{113}>{110} (fig. 6B)
	636.9	{111}>{100}>>{113}>{110}
	741.0	{110}>{113}
633 nm	637.0	{111}>{100}>{113}≈{110} (fig. 6C)
	648.1	{111}
	662.5	{100}>{111}>>{113}
	676.2	{100}≈{111}>>{113}
	681.1	{100}>{111}>{113}
	684.0	{110}>{113}
	718.2	{111}>{100}>{113}
	741.1	{110}>{113}>{100}>>{111}
780 nm	795.7	{111}
	815.1	{110}>{113}>{100}>{111} (fig. 6D)
	816.9	{111}
	823.8	{110}>{113}>{100}≈{111}
	828.8	{110}>>{113}
	833.0	{110}>>{113}
	843.2	{110}>{100}>{113}>{111}
	845.0	{110}>{113}>{111}>{100}
	849.4	{111}
	853.5	{110}>{113}>>{100}≈{111}
	855.6	{110}>{113}>{111}>{100}
	859.6	{110}>>{113}>{100}
	861.0	{110}>>{111}>{113}>{100}
	864.7	{110}>{113}>{100}≈{111}
	866.7	{110}>{113}>{111}
	873.4	{110}>{113}>{111}>{100}
	878.6	{111}>{100}≈{110}≈{113}
	884.6	{111}
	886.0	{111}
	889.1	{110}>{113}
	897.1	{110}>{111}>{113}>{100}
	898.6	{110}>{113}>{100}
	921.4	{111}
	931.7	{110}
	936.3	{110}
	939.4	{111}
	970.1	{111}

[a] *Baseline-corrected peak area used for comparison*

correlate with the four growth sectors visible in the DiamondView image (figure 4). The peak area intensity for the NV^- center is greatest in the {111} growth sector, nearly double its intensity in {100} and two orders of magnitude greater than in the {110} and {113} sectors. At 633 nm excitation, the GR1 peak at 741 nm was present in all four visible growth sectors. However, the GR1 intensity in {111} and {100} was less than half the GR1 intensity found in the {110} sector.

Meanwhile, the 780 nm excitation revealed the most peaks of any laser used for this study (table 2). Figure 6D shows the peak area distribution for the 815.1 nm peak. The four growth sectors seen in the DiamondView image (again, see figure 4) are visible in the PL image for the 815.1 nm peak area (figure 6D). For the 815.1 nm peak, the {110} sector had the greatest peak area intensity, an order of magnitude greater than in {113}. The peak area intensity in both {111} and {100} was an order of magnitude less than in the {113} sector. Many of the peaks observed using the 780 nm laser and reported in table 2 were most intense in the {110} sector.

DISCUSSION

The data in this study and in previous studies (e.g., Johnson et al., 2015; Dieck et al., 2015; Ardon and Loudin, 2016; Johnson and Myagkaya, 2017) show a clear correlation between the growth features observed in PL maps with DiamondView images. The strong correlation demonstrates the effectiveness of PL mapping in resolving the spatial distribution of optical defects in diamond. The visibility of growth features in the PL maps is a function of both the peak's intensity and its distribution. For example, in this study the 849.4 nm peak is only visible in the {111} growth sector (table 2). Accordingly, the remaining growth sectors cannot be identified using the 849.4 nm peak intensity. Therefore, it is likely that the 849.4 nm peak is preferentially incorporated in the {111} octahedral growth sector. Using similar reasoning, at least 10 peaks from this study are preferentially incorporated in {111} and two peaks in {110} (table 2).

The distribution of the 849.4 nm band also demonstrates the advantage of PL mapping over standard PL. If in a standard PL measurement the instrument operator unknowingly focused on the part of the table corresponding to the {110} sector, then the 849.4 nm peak would not be observed in the spectra. In the same instance, the intensity of the NV^- (637 nm) and NV^0 (575 nm) centers would be lower and the intensity of

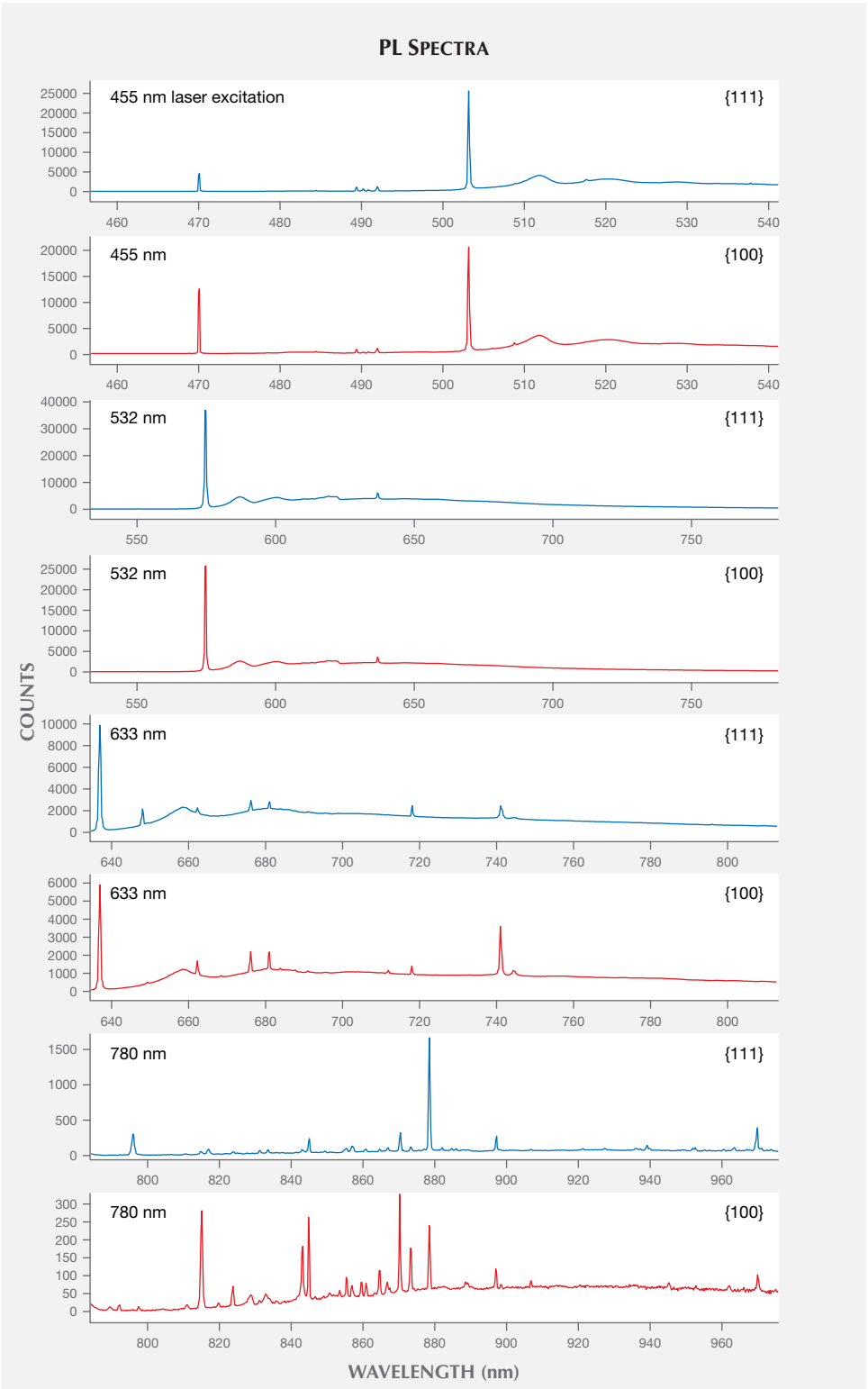

Figure 7. Average PL spectra for the {100} and {111} growth sectors. For each laser excitation, the spectra show that the abundance and intensity of optical defects varies between the {100} and {111} growth sectors.

GR1 (741 nm) would be higher than if the spectra were collected in the {111} sector. This is important to note because, as stated in Eaton-Magaña and Breeding (2016), determining some diamond color treatments relies on the "presence and absence of particular PL peaks." Therefore, PL mapping provides scientists

with a three-dimensional understanding of the diamond's optical defects, its PL intensity, and its spatial distribution.

Finally, to assess the effectiveness of the PL mapping technique introduced in this study, we can compare our data to previous studies that have assigned optical defects to particular growth sectors. The concept of optical defects being incorporated in a specific growth sector is well documented (van Enckevort and Lochs, 1988; Collins et al., 1990; Lawson et al., 1996; Welbourn et al., 1996; Zaitsev, 2001). For instance, the NV^- center is preferentially incorporated in the {111} octahedral sector in HPHT synthetic diamonds (van Enckevort and Lochs, 1988; Zaitsev, 2001). In agreement with the study presented by van Enckevort and Lochs (1988), our results show that the NV^- center is most intense in the {111} octahedral growth sector (table 2). Furthermore, the GR1 intensity was greatest in the {110} growth sector (also in table 2). Comparing the distribution of GR1 to that of the NV^- center, we see a nearly opposite distribution of the two defects. This is expected because a vacancy introduced in the {111} growth sector can readily combine with the available N to form the nitrogen vacancies (Burns et al., 1990). The correlation between our PL maps and the results from previous studies validates the effectiveness of using an EMCCD Raman imaging microscope for rapidly collecting PL maps.

CONCLUSIONS

Using a unique HPHT synthetic diamond of mixed type, our high-speed photoluminescence mapping technique produced images that reveal the intensity variations of PL features between growth sectors. The collected PL images, obtained in less than four minutes each, establish the usefulness of this method in understanding the preferential uptake of impurities and optical defects in diamond growth. We conclude that using an EMCCD Raman imaging microscope is an effective and efficient method for determining the distribution of optical centers in diamond and producing PL maps. This technique will allow scientists to rapidly collect and analyze PL maps in order to better understand the nature and formation of optical defects in diamond and evaluate new criteria for identifying treated and synthetic diamonds.

ABOUT THE AUTHOR

Mr. Loudin is a research associate in diamond advanced testing at GIA in New York.

ACKNOWLEDGMENTS

The author thanks Alexander Rzhevskii of Thermo Fisher Scientific for providing detailed information on the DXRxi EMCCD and instrument automation. The author also thanks A'Dhi Lall and Towfiq Ahmed of GIA's New York lab for collecting the FTIR spectra and acquiring the photo of the sample, respectively. In addition, the author would like to thank three anonymous reviewers, as well as Christopher M. Breeding of GIA in Carlsbad, for providing thoughtful comments and suggestions. The author is grateful to Paul Johnson and Wuyi Wang of GIA's New York lab for their continued support during the development of this PL mapping technique.

REFERENCES

Ardon T., Loudin L. (2016) Lab Notes: Evidence of focused beam irradiation in treated pink diamond. *G&G*, Vol. 52, No. 3, pp. 298–299.

Breeding C.M., Shigley J.E. (2009) The "type" classification system of diamonds and its importance in gemology. *G&G*, Vol. 45, No. 2, pp. 96–111, http://dx.doi.org/10.5741/GEMS.45.2.96

Burns R.C., Cvetkovic V., Dodge C.N., Evans D.J.F., Rooney M.-L.T., Spear P.M., Welbourn C.M. (1990) Growth-sector dependence of optical features in large synthetic diamonds. *Journal of Crystal Growth*, Vol. 104, No. 2, pp. 257–279, http://dx.doi.org/10.1016/0022-0248(90)90126-6

Collins A.T. (1982) Colour centres in diamond. *Journal of Gemmology*, Vol. 18, No. 1, pp. 37–75.

——— (1992) The characterisation of point defects in diamond by luminescence spectroscopy. *Diamond and Related Materials*, Vol. 1, No. 5-6, pp. 457–469, https://doi.org/10.1016/0925-9635(92)90146-F

——— (1999) Things we still don't know about optical centres in diamond. *Diamond and Related Materials*, Vol. 8, No. 8-9, pp. 1455–1462, http://dx.doi.org/10.1016/S0925-9635(99)00013-8

——— (2003) The detection of colour-enhanced and synthetic gem diamonds by optical spectroscopy. *Diamond and Related Ma-*

terials, Vol. 12, No. 10-11, pp. 1976–1983, http://dx.doi.org/10.1016/S0925-9635(03)00262-0
Collins A.T., Kanda H., Burns R.C. (1990) The segregation of nickel-related optical centres in the octahedral growth sectors of synthetic diamond. *Philosophical Magazine Part B*, Vol. 61, No. 5, pp. 797–810, http://dx.doi.org/10.1080/13642819008207562
Dieck C., Loudin L., D'Haenens-Johansson U. (2015) Lab Notes: Two large CVD-grown synthetic diamonds tested by GIA. *G&G*, Vol. 51, No. 4, pp. 437–439.
Eaton-Magaña S., Breeding C.M. (2016) An introduction to photoluminescence spectroscopy for diamond and its applications in gemology. *G&G*, Vol. 52, No. 1, pp. 2–17, http://dx.doi.org/10.5741/GEMS.52.1.2
Eaton-Magaña S., Shigley J.E. (2016) Observations on CVD-grown synthetic diamonds: A review. *G&G*, Vol. 52, No. 3, pp. 222–246, http://dx.doi.org/10.5741/GEMS.52.3.222
van Enckevort W.J.P., Lochs H.G.M. (1988) Photoluminescence tomography as a method to image point-defect distributions in crystals: Nitrogen-vacancy pairs in synthetic diamond. *Journal of Applied Physics*, Vol. 64, No. 1, pp. 434–436, http://dx.doi.org/10.1063/1.341212
Johnson P., Myagkaya E. (2017) Lab Notes: HPHT synthetic diamond with intense green color. *G&G*, Vol. 53, No. 1, pp. 96–98.
Johnson P., Moe K.S., D'Haenens-Johansson U., Rzhevskii A. (2015) Discovery and distribution of the $[Si\text{-}V]^-$ defect in HPHT-grown gem-quality diamonds. *Geological Society of America Abstracts with Programs*. Vol. 47, No. 7, p. 763.
Law B., Wang W. (2016) Lab Notes: CVD synthetic diamond over 5 carats identified by GIA. *G&G*, Vol. 52, No. 4, pp. 414–416.
Lawson S.C., Kanda H., Watanabe K., Kiflawi I., Sato Y., Collins A.T. (1996) Spectroscopic study of cobalt-related optical centers in synthetic diamond. *Journal of Applied Physics*, Vol. 79, No. 8, pp. 4348–4357, http://dx.doi.org/10.1063/1.361744
Moe K.S., D'Haenens-Johansson U., Wang W. (2015) Lab Notes: Irradiated green-blue CVD synthetic diamonds. *G&G*, Vol. 51, No. 3, pp. 320–321.
Moe K.S., Johnson P., D'Haenens-Johansson U., Wang W. (2016) Lab Notes: Largest blue HPHT synthetic diamond. *G&G*, Vol. 52, No. 1, pp. 74–75.
Wang W., Poon T. (2016) Lab Notes: Large blue and colorless HPHT synthetic diamonds. *G&G*, Vol. 52, No. 2, pp. 195–196.
Welbourn C.M., Cooper M., Spear P.M. (1996) De Beers natural versus synthetic diamond verification instruments. *G&G*, Vol. 32, No. 3, pp. 156–169, http://dx.doi.org/10.5741/GEMS.32.3.156
Zaitsev A.M. (2001) *Optical Properties of Diamond: A Data Handbook*. Springer-Verlag, Berlin.